Systematics of spin-polarized small Na clusters

K. Andrae, P.-G. Reinhard, E. Suraud
Institut für Theoretische Physik,
Universität Erlangen,
Staudtstrasse 7, D-91058 Erlangen, Germany
and
Laboratoire de Physique Théorique,
Université Paul Sabatier,
118 Route de Narbonne, F-31062 Toulouse, cedex,
France

January 3, 2007

Abstract

Inspired by recent experiments on fully spin polarized Na clusters, we perform a systematic survey of neutral Na clusters at all conceivable spin polarizations. We study the impact of spin state on ionic configuration, on global shape, and on optical response. For small clusters, the magic electronic shell at 4 spin-up electrons is a dominating feature leading to preferred binding for all clusters having four spin-up electrons (combined with 1 to 4 spin-down electrons). Such a preference fades away for larger systems where the unpolarized state is generally preferred.

1 Introduction

Clusters in contact with a medium display a rich variety of possibilities not accessible with merely free clusters. A typical example is here a medium consisting out of a large drop of liquid He. It provides a low-temperature laboratory for studies of various dynamical effects on small molecules and clusters [1]. It has also been used as a tool to produce free Mg clusters [2]. Accordingly, there exist several publications

investigating the cluster-medium interaction, see e.g. [3, 4]. A particularly interesting effect emerges, if Na is brought into contact with the drops. Sodium atoms can then form clusters on the surface and the high volatility of the drop acts as a criterion to select fully spin-polarized Na clusters [5]. A series of such clusters has been observed up to $N = 16$ [6]. We take these recent experiments as motivation for a theoretical survey of spin-polarized Na clusters. The aim of this paper is to investigate from a theoretical perspective the structure and optical response of small neutral Na clusters (up to $N = 10$) at all conceivable spin states. Selected examples of clusters with spontaneous spin-polarization had been studied in earlier publications [7, 8]. Here we aim at a more systematic survey going up to the extremes of fully spin-polarized systems. We use the same tools as in previous publications, namely (time-dependent) density-functional theory for electrons and simulated annealing for ionic structure optimization. The sequence of definite spins is produced by fixing the spin state of the cluster. The stability of fully spin-polarized configurations is checked by allowing the spins to vary freely.

2 Formal framework

2.1 Approach and computational scheme

The electron cloud of the clusters is described by density-functional theory at the level of the local spin-density approximation (LSDA) using the density functional of Ref. [9] which is known to perform reliably well also in the spin channel. We complement that by a self-interaction correction with the average-density approach (ADSIC) [10]. This provides correct ionization potentials and an appropriate asymptotic tail of the density. The coupling of ions to electrons is described by a local pseudo-potential which has been proven to yield correct ground state and optical excitation properties of simple sodium clusters [11]. The spin-orbit force is negligible for Na. This means that spin is totally decoupled from spatial properties and there is rotational invariance in spin space. It is to be expected that stationary states have collinear spin distributions and integer total spin. We have checked that by allowing non-collinear spin (for details see section 2.2) and we find indeed collinear configurations throughout. Thus we continue with computing the states with fixed total z-component of spin in collinear configurations. In that cases, there is one spin orientation throughout and its direction is arbitrary. Clusters are characterized then by their net polarization which is obtained as the sum of the single z-component $S_z = s_z$. A coupling to good total spin produces a sum of Slater states. This is what is called a correlated state. It goes outside the realm of density functional theory. Within LSDA we have at hand only the total

z-component $S = S_z$ and we take that to characterize the spin state of the system. It is to be noted that it is just that S_z which couples to an external magnetic field. We thus have an appropriate measure of the magnetic response of the cluster within LSDA, similar as it was studied before, e.g., in [7].

The electron wavefunctions are represented on an equidistant grid in three-dimensional coordinate space. The electronic ground state solution is found by iterative relaxation [13]. The electronic net spin is chosen at the initialization stage and stays unchanged throughout the relaxation. The ionic configurations are optimized by simulated annealing [14]. To compute the optical response, we propagate the electronic dynamics at fixed ionic configuration. Propagation is done with time-dependent LSDA (TDLSDA) using the time-splitting method [15]. To compute the spectral distributions, we perform a spectral analysis after the TDLDA propagation [16, 17]. This means that we initialize the dynamics by a small instantaneous boost of the center-of-mass of the electron cloud. The dipole moment is recorded during time evolution. A Fourier analysis into frequency domain then finally yields the spectral strength. For all technical details see the review [18].

The global shape of the cluster is characterized by the r.m.s. radius and the dimensionless quadrupole moments $\alpha_{2\mu}$ recoupled to the total deformation β and triaxiality γ. The various quantities read,

$$r = \sqrt{\frac{\langle r^2 \rangle}{N}} \ , \ \beta = \sqrt{\alpha_{20}^2 + 2\alpha_{22}^2} \ , \ \gamma = \mathrm{atan}\frac{\sqrt{2}\alpha_{22}}{\alpha_{20}} \ , \ \alpha_{2m} = \frac{4\pi}{5}\frac{\langle r^2 Y_{2m} \rangle}{N r^2} \ . \qquad (1)$$

These equations can be read in two ways: for electrons, $\langle ... \rangle$ is the moment of the density $\rho_{\mathrm{el}}(\mathbf{r})$ and $N \equiv N_{\mathrm{el}}$, while for ions, one considers the classical moment $\langle f(\mathbf{r}) \rangle = \sum_I f(\mathbf{R}_I)$ and identifies $N \equiv N_{\mathrm{ion}}$. The leading and most robust quantity is the r.m.s. radius. Its relative variation is limited as we will see. The total deformation β is still a robust quantity showing, however, large variations in the range 0–1/3. The triaxiality γ is more special. One has to keep in mind that it is well defined only for sufficiently large deformation, typically $\beta \gtrsim 1/10$. It is undefined for $\beta = 0$ and only vaguely defined for small β.

Variation of the spin composition is the major objective of that paper. We need a compact notation to characterize that and we will denote it by an upper index. The notation $\mathrm{Na}_N^{N_\uparrow N_\downarrow}$ stands for a Na_N cluster with $N_\uparrow$ spin-up electrons and $N_\downarrow$ spin-down electrons. Without loss of generality, we sort $N_\uparrow \geq N_\downarrow$. The total electron number combines to $N = N_\uparrow + N_\downarrow$. The spin state is characterized by the net spin $S = N_\uparrow - N_\downarrow$. Note that we will count spin in units of $\hbar/2$ throughout this paper.

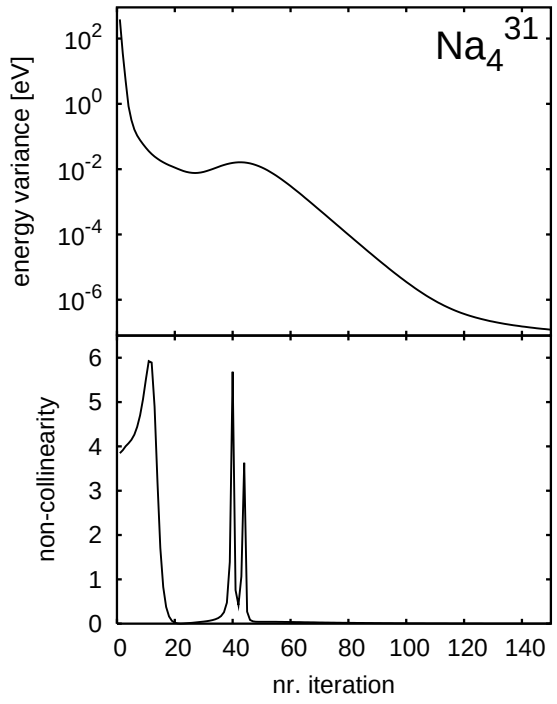

Figure 1: Evolution of energy variance $\Delta E = \sqrt{\sum_\alpha (\varphi_\alpha | \hat{h}^2 - \bar{h}^2 | \varphi_\alpha)}$ (upper panel) and non-collinearity (lower panel) during iteration towards the electronic ground state configuration. The non-collinearity is defined in eq. (2). Test case of the cluster $\mathrm{Na}_4^{(31)}$ in the final configuration with three spin-up and one spin-down electron.

2.2 Collinearity

The explicit treatment of spins allows still two options: one can assume that all spins are aligned (collinear) or one allows for non-collinearity as it is necessary, e.g. for magnetic materials [12]. Materials with negligible spin-orbit coupling, as e.g. Na, should have always collinear spin. Nonetheless, we have checked that in detail using the code of [12]. For a handful of test cases, we initialize the electronic configuration in a non-collinear state and watch the evolution of that during ground-state iteration. We always find a quick convergence towards collinear configurations. One example is shown in figure 1. The energy variance in the upper panel serves to demonstrate the overall convergence pattern. It remains to quantify the non-collinearity in one simple number. To that and, we evaluate the spin-orientation σ_α for each electron state α

seperately, compute the angle between all pairs of electrons, and finally add up the quadratic deviations. This yields the "non-collinearity" as

$$\Delta\sigma^2 = \sum_{\alpha\beta} \sin^2(\sigma_\alpha, \sigma_\beta) \ , \ \sin^2(\mathbf{a}, \mathbf{b}) = 1 - \frac{(\mathbf{a}\cdot\mathbf{b})^2}{\mathbf{a}^2\mathbf{b}^2} \ , \ \sigma_\alpha = (\varphi_\alpha|\hat{\sigma}|\varphi_\alpha) \ , \tag{2}$$

where $\hat{\sigma}$ is the vector of Pauli spin matrices, i.e. the spin in units of $\hbar/2$. That measure is shown in the lower panel of figure 1. One sees a quick convergence to collinearity, an interesting interludium where non-collinearity pops up again to foster a quick transition into a better configuration, and finally a stable collinear state. All cases studied showed the same stable final convergence to a collinear configuration. Thus we use the code with (much faster) thoroughly collinear handling of spin.

However, the non-collinear confgurations become important for detailed studies of spin stability. Each spin state is conserved for the present energy functional. It is only by perturbations, namely a small sin-orbit coupling in the pseudo-potentials or external magnetic fields, that the spin states can mix and undergo transitions which possibly run through non-collinear configuration as transitional stages. Such studies go beyond the scope and limitations of the present paper. We will adopt, in accordance with experimental claims [6], that the spin states once prepared stay stable for the necessary analyzing time.

3 Results and Discussion

3.1 Details of configurations and shapes

In a first round we investigate the structure of polarized Na clusters. For a given size N, we can have $N/2+1$ different spin states $S = N, N-2, N-4, ...,$ mod $(N, 2)$. For each spin state $S = N_\uparrow - N_\downarrow$ kept fixed, we optimize the ionic structure. As a consequence, we generate all ground state configurations for systems (N, S) with $N = 3, .., 8, 10$ and all S as given above. One can now imagine that a given ground state for (N, S) may undergo a sudden spin flip $S \to S'$. The ions readjust to the new S' very slowly. Electronic relaxation is much faster. We thus obtain a transient cluster with ionic structure of (N, S) but electronic structure readjusted to S'. The following figures show results for all the ground states as well as for all possible combinations to transient states $S \to S'$. The ionic configurations used are distinguished by line types, see figure captions. The actual electronic spin is given on the abscissa (in electronic spin unit $(\hbar/2)$).

Figures 2–8 show the global properties (cohesive energy, radius, deformation, IP) of all considered clusters together with a graphical illustration for the ionic structures.

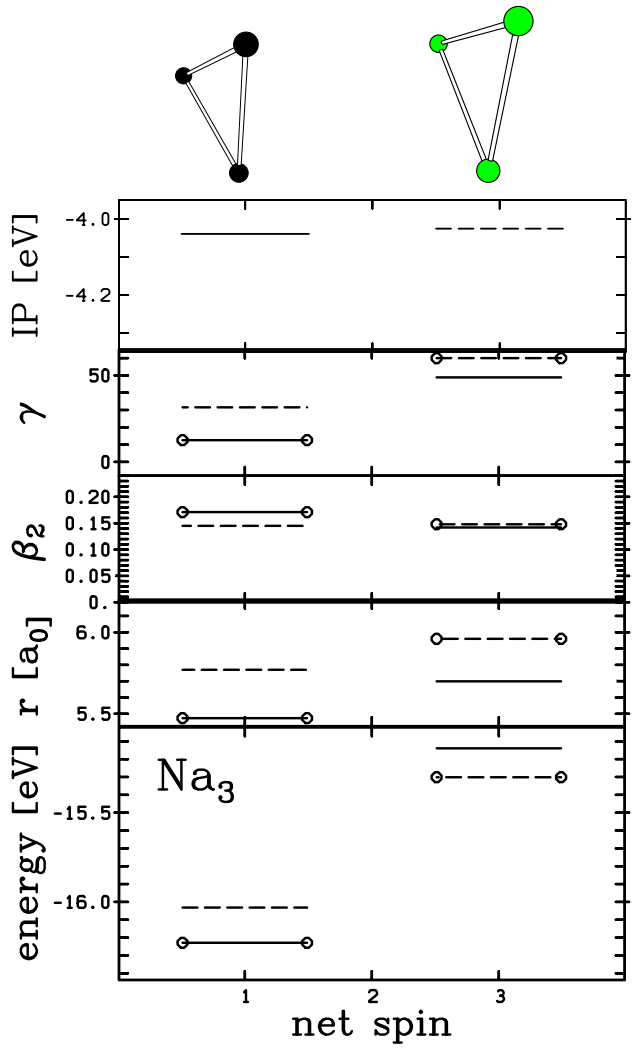

Figure 2: Global properties of Na_3 in various spin states: Lower panel = binding energy, second lower panel = r.m.s. radius, middle panel = total quadrupole deformation, second upper panel = triaxiality, uppermost panel = ionization potential (IP). The shape parameters are related to the electronic distribution and defined in eq. (1). On top of the panels, the ionic configurations which had been optimized for given electronic net spin are shown. The panels show results where all possible net-spins are computed in connection with all possible configurations. The line type indicates the ionic configuration: full line $\leftrightarrow$ optimized for spin=1, dashed $\leftrightarrow$ optimized for spin=3. The (preferable) cases where actual electronic net-spin coincides with the spin for which the ionic configuration has been optimized are indicated by circles. The corresponding ionic configurations are shown on top of the panels.

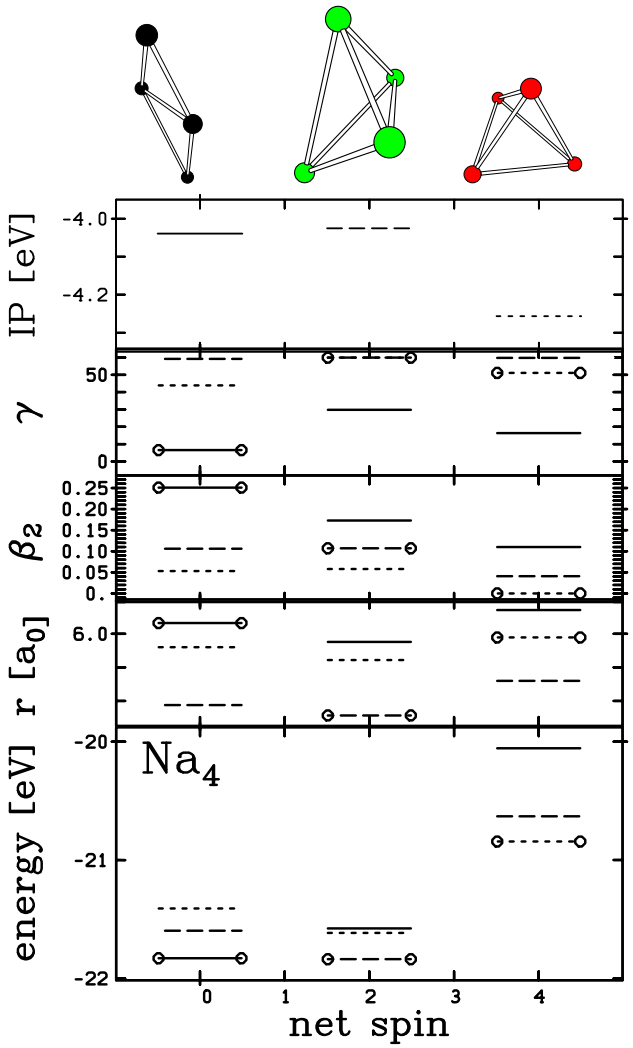

Figure 3: As figure 2 for the cluster Na_4. The assignment of line types to ionic configuration are: full line $\leftrightarrow$ optimized for spin=0, dashed $\leftrightarrow$ optimized for spin=2, dotted $\leftrightarrow$ optimized for spin=4.

These figures are all built according to the same scheme and we discuss them in one stroke. Looking at the binding energies, we see (with few exceptions) that the energies for different ionic configurations but same net spin gather in densely packed small blocks while large energy shifts emerge when changing electronic net spin. The binding energies thus depend predominantly on the electronic net spin while details of the ionic configuration make less effect, although there can be substantial ionic rearranegements, particularly for the smaller clusters. Questions of spin stability may thus be discussed in a first step on grounds of electronic dynamics (as done to some extend in section 2.2). The ionic rearrangement follows in a second step. This view is not only suggested by energetic considerations but also for reasons of time scale. Electronic transitions run at the order of a few fs while ionic motion takes hundreths of fs.

The radii basically follow the trends of the binding energy, deeper binding relates to smaller radii. This holds strictly for the cases where electrons and ionic configuration are simultaneously optimized (bars distinguished by circles in the figures). The other combinations of electron spin and ionic configurations show variations which are larger than the respective variations in energy and which can, in contrast to the energy, vary in both directions around the optimized result. The deformation parameters β and γ also show large variations with ionic configuration at given net spin. These variations are as large, often even larger, as the changes with net spin. This happens because the electrons like to follow the given ionic shape in order to minimize the Coulomb energy [20].

The relation between electronic and ionic shape is visible in figure 7. It shows the shape parameters for both species (ionic with stars, electronic with circles). Ionic and electronic radii follow precisely the same trend. But the electronic radius is systematically larger than the ionic radius. This is due to the much smoother electronic surface distribution. The deformation parameters β and γ coincide for electrons and ions. This demonstrates that the electrons follow the ionic distribution or vice versa. It becomes fully obvious when looking at the β and γ across the various spins and comparing results only for the same line type which means the same ionic configuration. In this way, the results show much less variation.

Let us now concentrate on the simultaneously optimized configurations (indicated by circles in the figures), i.e. the electronic plus ionic ground states at given spin, and let us go through the examples top down, i.e. from the largest sample to the smallest. Figure 8 for Na_{10} shows the expected trends. The unpolarized configuration is the preferred one and there is a steadily increasing energy towards the fully polarized case. Two details go a bit against these general trends. First, the case with net spin 2 has very small energy difference to the spin 0 ground state. This configuration consists out of 6 spin-up with 4 spin-down electrons and the 4 electrons of one spin constitute

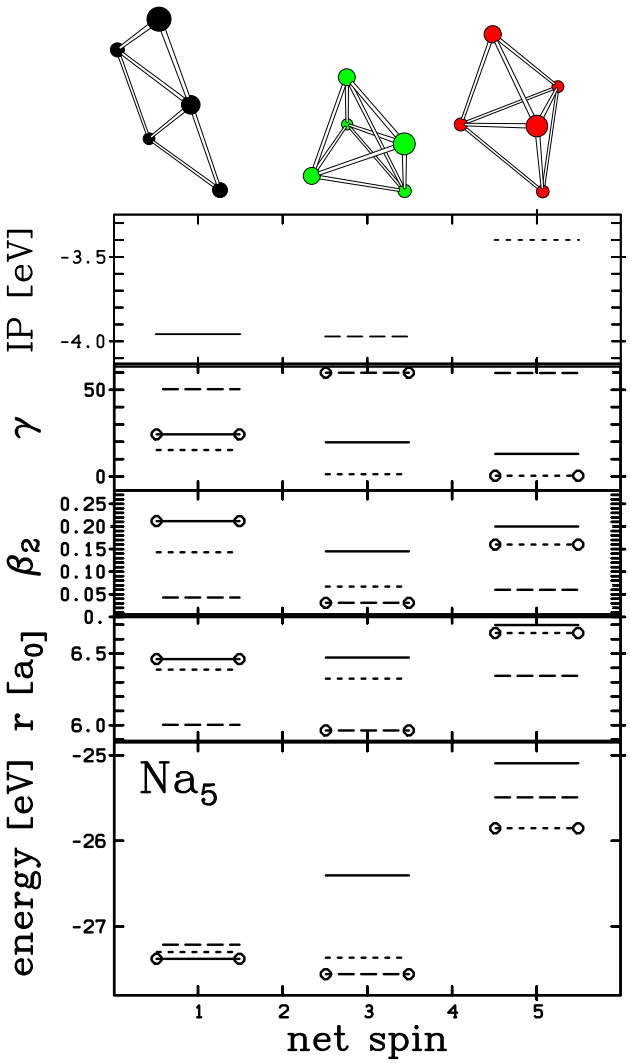

Figure 4: As figure 2 for the cluster Na_5. The assignment of line types to ionic configurations are: full line $\leftrightarrow$ optimized for spin=1, dashed $\leftrightarrow$ optimized for spin=3, dotted $\leftrightarrow$ optimized for spin=5.

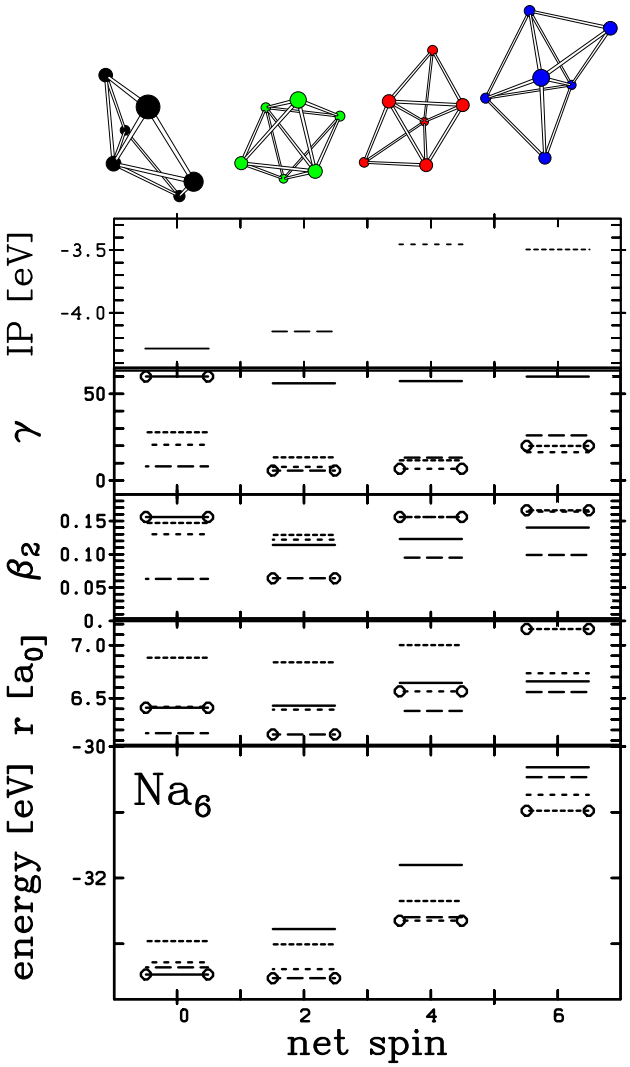

Figure 5: As figure 2 for the cluster Na_6. The assignment of line types to ionic configurations are: full line $\leftrightarrow$ optimized for spin=0, dashed $\leftrightarrow$ optimized for spin=2, dotted $\leftrightarrow$ optimized for spin=4, fine-dotted $\leftrightarrow$ optimized for spin=6.

a magic electron shell. The slight "magicity" can also be read off from the dip of the deformation β at spin 2. The second detail concerns the state with spin 10. The very small β there indicates a nearly spherical shape. Again we meet a magic number where 10 electrons of one spin form a closed shell. In this case, the "magicity" is not strong enough to be honored by the binding energy. But it suffices to drive the spherical shape.

The results for Na_8 in figure 7 come even closer to what one would have naively expected. There is an almost equidistant rise in energy and radius with increasing spin. But mind that we have here an enhanced preference of the unpolarized state by a fully developed magic electron number at spin 0, namely 4 electrons spin-up and 4 spin-down. This is corroborated by the fact that this system again has low β and is thus close to spherical shape. The case of Na_7 in figure 6 is much similar to Na_8. No surprise, because the lowest spin 1 coincides again with the magic electron closure of the 4 spin-up electrons. Comparing the cases Na_8 and Na_7 with Na_{10}, we conclude that there is a general trend toward unpolarized systems, but that shell closures can change the picture in detail. That means that small net spin may emerge as ground state configuration if one spin species has a magic electron number and the other species just suffices to compensate to net spin 2, or 3 respectively. This effect will become more obvious for the smaller systems.

The example of Na_6 shown in figure 5 is the first case where shell closure is compensating the trend to zero polarization. The global ground state happens to be configuration with spin 2, not surprisingly just the case covering a magic shell of 4 spin-up electrons. The radius follows the trend of the energy, and last not least, the "magicity" is again indicated by a drop in deformation β. The situation is similar again in the next lower Na_5 cluster. The ground state is here with spin 3 because this contains the magic shell of 4 spin-up electrons. In both examples, however, the notion of a ground state configuration has to be taken with a grain of salt. The energy difference to the minimum spin state is extremely small. A clear clut decision between ground state and first isomer may be beyond the reliability of LSDA. In any case, the qualitative result will persist, namely that the spontanously spin polarized state is competitive with the minimum spin state. And this has interesting consquences on the magnetic response as was discussed in [7].

The fully spin polarized Na_4 is again close to spherical in compliance with the shell closure at $N = 4$ spin-up electrons. However, the energetically favored ground state configuration is ${Na_4}^{31}$ having net spin 2. The price for full spin polarization is here higher than the gain from shell closure. Finally, nothing peculiar can be seen for the smallest system Na_3. It is necessarily a flat object and thus has always a certain deformation. Note that triaxiality γ is not so well defined and thus fluctuates for such a small system.

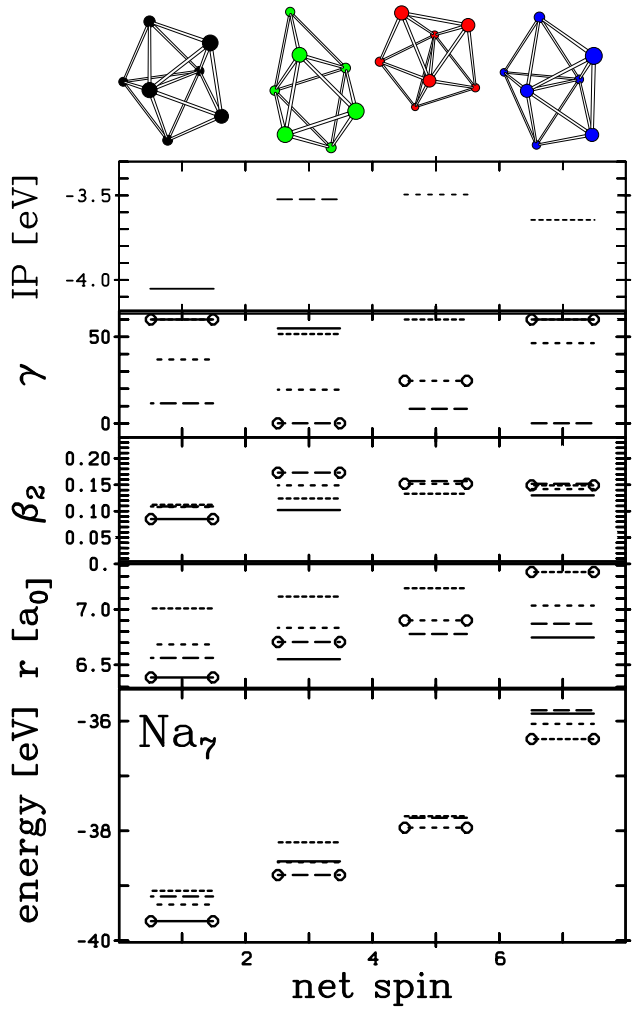

Figure 6: As figure 2 for the cluster Na_7. The assignment of line types to ionic configurations are: full line $\leftrightarrow$ optimized for spin=1, dashed $\leftrightarrow$ optimized for spin=3, dotted $\leftrightarrow$ optimized for spin=5, fine-dotted $\leftrightarrow$ optimized for spin=7.

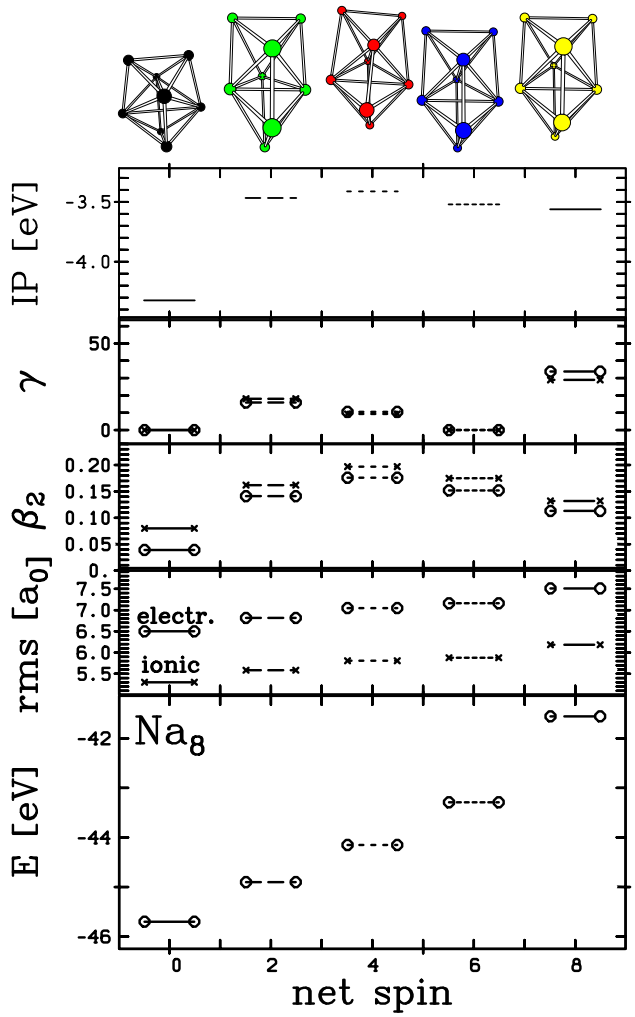

Figure 7: Global properties of Na_8 in various spin states: Lower panel = binding energy, second lower panel = r.m.s. radius, second upper panel = total quadrupole deformation, upper panel = triaxiality. The shape parameters are shown for the electronic distribution (lines embraced by circles) as well as for the ionic configuration (lines embraced by stars). They are defined in eq. (1).

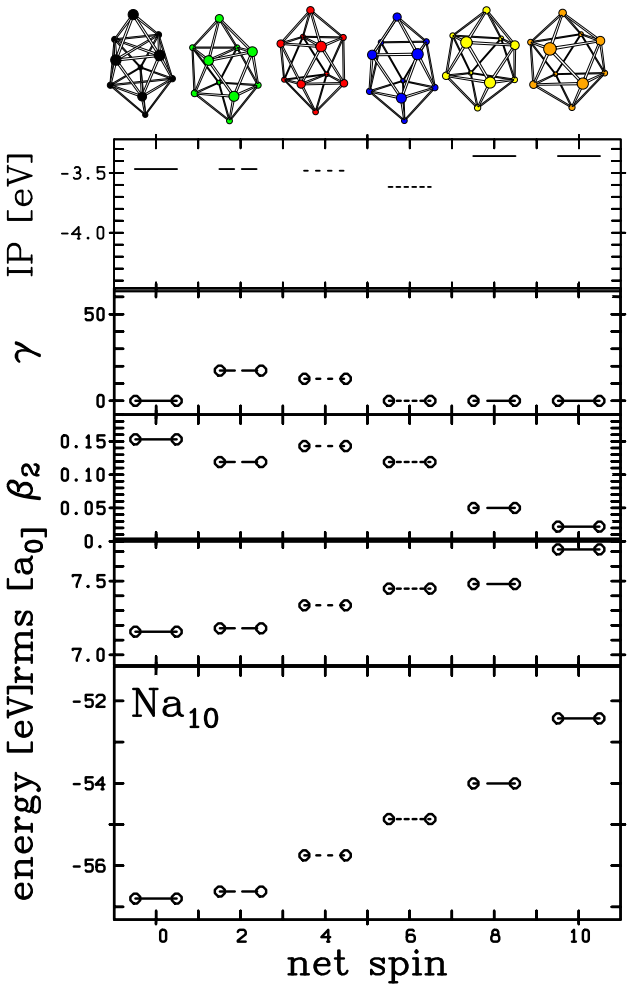

Figure 8: As figure 7 for the cluster Na_{10}.

The small clusters Na_4 and Na_5 show a strong dependence of the shape on spin. The unpolarized configurations are planar while the spin polarized states extend in three dimensions. This is due to the drive of the $N_{\rm spinup} = 4$ shell to sphericity. The differences in shape become less dramatic with increasing N. But one still has for any N the influence of magic $N_{\rm spinup}$ producing minima in β. The effect is obvious for the $N_{\rm spinup} = 4$ shell. But one sees it also on the β from the softer $N_{\rm spinup} = 10$ shell. There is a pronounced minimum for Na_{10}. For Na_8, the maximum β is precisely in between 4 and 10 whereas the fully polarized Na_8 clearly shows the descend of β toward the magic shell.

Besides total energies, figures 2–8 provide also the ionization potentials (IP) of the various spin configurations. The IP characterizes the stability of a system against removal of an electron. The magic shell $N_{\rm spinup} = 4$ is clearly visible. The overall pattern show the typical stepping up above at $N_{\rm spinup} = 4$ because the $1p$ state is fully occupied and the less well bound $1d$ state is going to become filled. The spin-saturated full-shell case $(N, N_{\rm spinup}) = (8, 4)$ is best bound. However, the differences to all others cases are very small.

A word is in place here about Hund's rules. These are formulated for atoms and they state that electrons in an open shell arrange themselves into a maximal spin-polarization to render the ground state non-degenerate. Clusters have an alternative, and more effective, way to arrange an unambiguous ground state, the Jahn-Teller effect, i.e. they drive into a deformation for which the electron occupation is unique. The two mechanisms compete and the Jahn-Teller deformation usually wins. Still, there are occasionally spin polarized isomers in clusters with truly triaxial shapes [7, 35]. These previous studies considered only small polarization up to net spin two. The present investigation goes up to any spin and reveals that shell closures for spin-polarized systems add an extra preference for electron number 4 (and 10) in one spin species. The extra binding leads to spin polarized ground states in very small Na clusters. It is so to say Hund's rules enhanced by shell effects.

3.2 Optical response

It is also interesting to investigate the key feature of cluster excitations, namely the optical response of polarizd clusters. Thus we investigate the dipole strength of the various clusters in our sample. Thereby we confine considerations to ionic configurations which are relaxed for given net spin. Figure 9 shows the dipole spectra all in the same manner for a selection of two clusters and configurations. The dipole strengths are evaluated along the principal axes which are usually very close to the optical axes of the clusters (the optical axes are those for which the dipole response tensor is diagonal). The comparison of spectra can be helpful to discriminate differ-

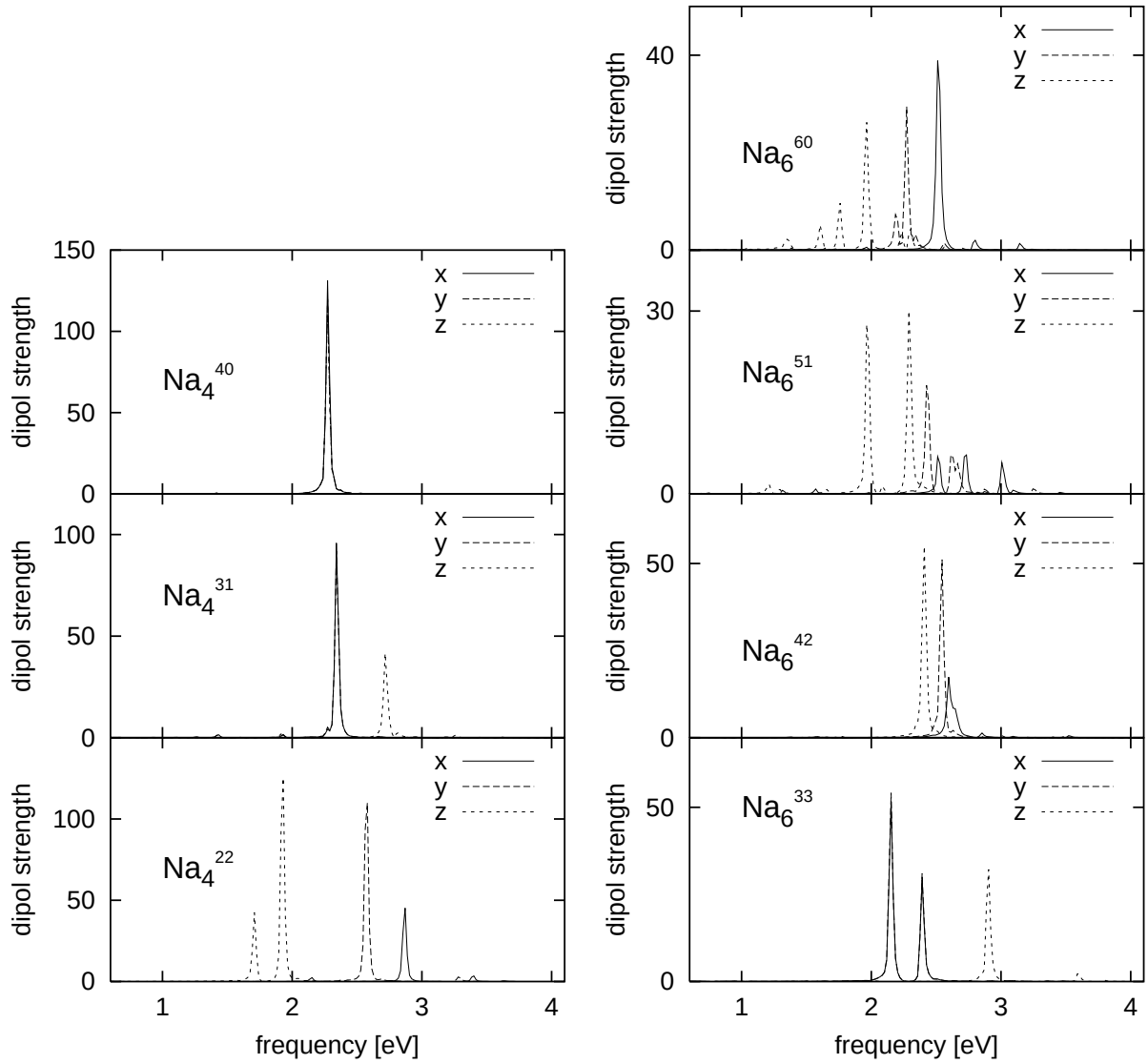

Figure 9: Dipole strengths along the three principle axes for the various spin-polarized states of Na_4 (left) and Na_6 (right) with polarization as indicated by the upper index.

ent spin states where they may compete in practice. The case becomes of course a bit academic for the high lying isomers because these are quickly destabilized by any additional excitation.

Before starting the detailed discussion, let us briefly recall the basic features of dipole spectra in metal clusters [18, 21]. The average position is roughly estimated by the Mie surface plasmon frequency. The total strength (according to the dipole sum rule) is contained to about 90% in the Mie plasmon resonance which can be very well computed in purely collective models [21, 26, 27]. The remaining strength is found in secondary surface plasmons and to a lesser extend in the volume plasmon. There are two mechanisms which produce a spread of the spectra around the average surface plasmon frequency. The global quadrupole deformation of the cluster leads to a splitting of the plasmon which can still be described at a collective level. The oscillations along the elongated axes are red shifted while those along the squeezed axes are blue shifted [28]. This deformation splitting is an important tool for assessing the deformation of small clusters [29, 30, 31]. The other source of spectral broadening is due to the coupling of the resonance to nearby one-particle-one-hole $1ph$ state. It is called Landau fragmentation because it is the finite systems analogue of Landau damping in the electron gas of a plasma. This effect sensitively depends on the details of the shell structure. As a rough rule one can say that Landau fragmentation becomes increasingly important the larger the clusters [21, 32]. For small clusters it plays a role in connection with broken parity symmetry [18].

In the following we discuss figure 9. We do also comment briefly on the results and trends obtained for other clusters even if the corresponding spectra are not displayed here. There are of course large differences concerning the degree of splitting or fragmentation, as a function of size and spin. The cleanest plasmon peaks are found systematically whenever the magic $N_{\mathrm{spinup}} = 4$ is involved which happens for the configurations (not all of them are shown here) $Na_4{}^{40}$, $Na_5{}^{41}$, $Na_6{}^{42}$, $Na_7{}^{43}$, and $Na_8{}^{44}$. These systems have all been identified in subsection 3.1 as being nearly spherical and accordingly there is no deformation splitting. Moreover, these configurations seem to be particularly stable as we see no or very little Landau fragmentation. The same clean plasmon peak is seen for the next magic $N_{\mathrm{spinup}} = 10$ in the spectrum of $Na_{10}{}^{100}$.

More or less fuzzy spectra are seen for the systems without shell closures. Let us consider the various pattern of deformation splitting and of Landau fragmentation for the various spin states of Na_6 (and please compare with the shapes as shown in figure 5). This example nicely covers all variants. The unpolarized cluster $Na_6{}^{33}$ is axially symmetric oblate ($\gamma = 60^o$). And accordingly the x- and y modes are degenerate. They are in the average red shifted relative to the z mode. This is the expected deformation splitting. However, one sees two peaks for the x-y-modes. This is a fragmentation caused by coupling to a detailed $1ph$ state. The $Na_6{}^{42}$ has a magic

electron shell. It is nearly spherical and correspondingly all modes gather around the same frequency. In fact, just for Na_6 sphericity is least perfect and thus we see a small remainder of deformation splitting. The cluster ${Na_6}^{51}$ is nearly cylindrically symmetric prolate. Thus x- and y- modes stay close to each other while the center of the z-mode is strongly red-shifted relative to that. (Remind that it was blue-shifted for the oblate case.) All three modes are slightly fragmented by coupling to $1ph$ states. Finally the cluster ${Na_6}^{60}$ is truly triaxial ($\gamma = 20^0$). And we see indeed a splitting into three distinct center frequencies for the three directions. Additionally, there is some Landau fragmentation for the z-mode. Altogether, we see that the simple rules of deformation splitting are well observed. The same holds for all other examples. The amount of Landau fragmentation is hard to predict in general terms. But the tendency that well bound magic shapes have less fragmentation is confirmed. The overall trend of average frequency with radius cannot easily be read off from the sometimes much split and fragmented spectra. Looking at the sequence a bit longer, one can see through the fuzzy pattern the expected trend, namely that the largest radius (${Na_6}^{60}$) has lowest frequency and the smallest radius (${Na_6}^{42}$) has the highest frequency. Similar observations can be made for all other spectra.

At second glance, we see in several spectra tiny spots of strength just above 1 eV. Take, for example, Na_6 in figure 9. The spectrum is absolutely empty below 2 eV for the unpolarized state ${Na_6}^{33}$. A hint of strength at 1.5 eV shows up in ${Na_6}^{42}$. It is better visible at the higher spin states where it finally resides around 1.2-1.3 eV. Previous studies have shown that small Na clusters possess spin-dipole modes around 1 eV and that spin-polarized clusters show cross talks between dipole and spin-dipole modes [33, 34]. We have checked that the small strength above 1 eV seen here is indeed due to cross talk with the spin-dipole mode.

Checking from that viewing angle figure 9 again, we see that the low lying strength in the fully polarized clusters differs very much for the various systems in the sample. The point is that the spin-dipole modes and the Mie plasmon mode in the dipole channel differ very much in their collectivity. Unlike the Mie plasmon mode, the spin-dipole experiences only a small residual Coulomb interaction (because the shifts of spin-up cloud and spin-down cloud go into opposite directions). It resides practically at pure $1ph$ energies. The $1ph$ energies, in turn, are determined by the spectral gap at the Fermi energy (HOMO-LUMO gap). And this gap depends on shell structure. Magic electron numbers, N=4 and 10, have a larger gap than intermediate systems. There is no low-lying strength in ${Na_4}^{40}$ and ${Na_{10}}^{100}$ while pronounced low lying states appear in the mid shell region.

4 Conclusions

We have investigated from a theoretical perspective the properties of small Na clusters at systematially varied spin polarization. We used as tool density-functional calculations at the level of the local-density approximation together with local pseudopotentials for the coupling of Na ions to the valence electrons. In a first step, we have checked possible non-collinearity of the spins. We find always fully collinear electron configurations for this simple material Na.

Electronic and ionic structure for small clusters has been discussed as well as optical response. Fully spin polarzed clusters display also a sequence of magic electron numbers which are just half of the magic numbers of spin saturated Na clusters. In our sample, we see the impact of the magic $N_{\rm spinup} = 4 = 8/2$ and Nspinup $= 10 = 20/2$. at various places. Magic $N_{\rm spinup}$ drive the system to minimum deformation, minimal radii, and relatively lower energies. As a consequence, several clusters show a large rearrangement of the ionic configuration when changing spin polarization.

We have also investigated optical response because it might provide a useful indicator of the underlying spin and ion structure. For the small clusters studied here, unpolarized systems show clean Mie plasmon resonances with a collective splitting directly related to the quadrupole deformation while the spectra of spin-polarized clusters show occasionally more fragmentation due to cross talk with spin modes.

The question of the life-time for highly spin-polarized clusters remains beyond the scope of this paper. It will be attacked in a next step.

Acknowledgments: This work has been supported by the French-German exchange program PROCOPE, contract number 99074, by Institut Universitaire de France, by the CNRS programe "Matériaux" (CPR-ISMIR), and by a Gay-Lussac prize. The authors furthermore acknowledge fruitful discussions with F. Stienkemeier.

References

[1] J.P. Tonnies, A.F. Vilesov, K.B. Whaley, Phys.Today **54** (2001) 31

[2] T. Döppner, Th. Diederich, J. Tiggesbäumker, K.H. Meiwes-Broer", Eur.Phys.J. D, **16** (2001) 13

[3] P. Leiderer, Z.Phys. B **98** (1995) 303

[4] F. Anciletto, E. Cheng, M.W. Cole, F. Taigo. Z.Phys. B **98** (1995) 323

[5] F. Stienkemeier, A.F. Vilesov, J.Chem.Phys. **115** (2001) 10119

[6] C. P. Schulz, P. Claas, D. Schumacher, and F.Stienkemeier, Phys.Rev.Lett. **92** (2004) 013401

[7] C. Kohl, B. Fischer, P.-G. Reinhard, Phys.Rev. B **56** (1997) 11149

[8] C. Kohl, S.M. El-Gammal, F. Calvayrac, E. Suraud, P.-G. Reinhard, Eur.Phys.Journ. D **5** (1999) 271

[9] J. P. Perdew and Y. Wang, Phys. Rev. B **45** (1992) 13244

[10] C. Legrand, E. Suraud, P.-G. Reinhard, J. Phys. B **35** (2002) 1115

[11] S. Kümmel, M. Brack, P.-G. Reinhard, Eur. Phys. J. D **9** (1999) 149

[12] C. Kohl, G.F. Bertsch, Phys.Rev. B **60** (1999) 4205

[13] V. Blum, G. Lauritsch, J.A. Maruhn, P.-G. Reinhard, J. Comp. Phys. **100** (1992) 364

[14] C. Kohl, PhD thesis, Erlangen 1997

[15] M.D. Feit, J.A. Fleck, A. Steiger, J.Comp.Phys. **47** (1982) 412

[16] K. Yabana, G.F. Bertsch, Z.Phys. D **42** (1997) 219

[17] F. Calvayrac, E. Suraud, P.-G. Reinhard, Ann.Phys. **254** (N.Y.) (1997) 125

[18] F. Calvayrac, P.-G. Reinhard, E. Suraud, C. Ullrich, Phys.Rep. **337** (2000) 493

[19] M. Brack, Rev.Mod.Phys. **65** (1993) 677

[20] B. Montag, P.-G. Reinhard, Phys.Rev. **B51** (1995) 14686

[21] P.-G. Reinhard, O. Genzken, M. Brack, Ann.Phys. (Leipzig) **5** (1996) 576

[22] B. Montag, P.-G. Reinhard, J. Meyer, Z.Phys. **D32** (1994) 125

[23] S. Kümmel, M.Brack, and P.-G. Reinhard, Phys.Rev. B **62** (2000) 7602

[24] T. Diederich, T. Döppner, J. Tiggesbäumker, K.-H. Meiwes-Broer, Phys.Rev.Lett. **86** (2001) 4807

[25] Ll. Serra, P.-G. Reinhard, E. Suraud, Euro.Phys.J. D **18** (2002) 327

[26] M. Brack, Phys. Rev. B **39** (1989) 3533

[27] P.-G. Reinhard, M. Brack, Phys. Rev. **A41** (1990) 5568

[28] W. Ekardt, Z. Penzar, Phys.Rev. B **43** (1991) 1331

[29] K. Selby, M. Vollmer, J. Masui, V. Kresin, W.A. de Heer and W.D. Knight, Phys. Rev. B**40** (1989) 5417

[30] P. Meibom, M. ⊘stergärd, J. Borggreen, S. Bjornholm and H.D. Rasmussen, Z. Phys. D**40** (1997) 258

[31] H. Haberland and M. Schmidt, Eur. Phys. J. D**6** (1999) 109

[32] V. O. Nesterenko, W. Kleinig, P.–G. Reinhard, Euro.Phys.J. D **19** (2002) 57

[33] L. Mornas, F. Calvayrac, P.-G. Reinhard, E. Suraud, Z.Phys. **D38** (1996) 73

[34] C. Kohl, S.M. El-Gammal, F. Calvayrac, E. Suraud, P.-G. Reinhard, Eur.Phys.Journ. D **5** (1999) 271

[35] C. Kohl, B. Montag, P.-G. Reinhard, Z. Phys. D **35** (1995) 57

[36] M.E. Garcia, G.M. Pastor, K.H. Benneman, Phys.Rev.Lett. **67** (1991) 1142